Warpage of rubber pressed composites

Sebastiaan Wijskamp, Edwin Lamers, Remko Akkerman & Erik van de Ven
Universiy of Twente (UT), The Netherlands
Faculty of Engineering
Department of Applied Mechanics and Plastics Engineering
Composites Group
e-mail: s.wijskamp@ctw.utwente.nl

ABSTRACT

The rubber pressing process is applied for the rapid production of thermoplastic composite products. However, rubber pressed products show geometrical distortions, such as warpage, due to process-induced residual stresses. It is believed that these stresses build up as a result of the large thermal gradients that are present during consolidation. An experimental study is performed to measure the curvature after rubber pressing of initially flat woven fabric glass/PPS composite panels. A material model is proposed that incorporates the solidification of the composite in order to predict the residual stresses and the warpage due to inhomogenous cooling. The model is employed in Finite Element simulations of the rubber pressing process. The simulations are compared to the experimentally obtained curvatures. It shows that inhomogeneous cooling has a minor effect on the warpage in this case, and that another mechanism is present.

KEYWORDS: **thermoplastic composites**, **warpage, rubber press forming, process-induced stress**

1. INTRODUCTION

Thermoplastic composite systems offer a well-known advantage over composites based on a thermosetting resin: the absence of a time-consuming chemical reaction allows for the relatively fast production of complex product shapes. The simplicity of the forming principle – reheating, shaping and cooling – offers a good basis for automation of the production processes involved with thermoplastic composites, making them commercially competitive to the relatively cheap thermosetting composites.

In the recent years, a number of relevant production processes has been developed, such as diaphragm forming, matched die forming, deep drawing and rubber pressing. These processes generally involve the reheating of the pre-consolidated laminate above its melting temperature, transfer to the die or tool, consolidation of the shaped laminate to a temperature at which it is solid and finally release and further cooling to the room temperature. In the particular case of rubber pressing, the shaping and consolidation take place between a rigid steel tool and a deformable rubber mould that is driven by a press, see Figure 1. The rubber pad can be configured as a simple block, or may be negatively shaped to allow for more complex product geometries. The process has the advantage over, for example, matched die forming that there is a nearly hydrostatic pressure on the product, even for small radius corners. A second feature of the process is the relatively low tooling costs; the steel tool can be used to cast the rubber mould.

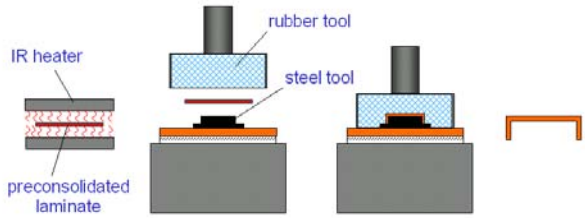

Figure 1. Sketch of the rubber pressing process.

A drawback of the production processes mentioned is the generally highly unbalanced thermal and mechanical loading of the composite during forming. As a result, the final product shows distortions such as warpage of intended flat parts. An example of a rubber pressed product is shown in Figure 2.

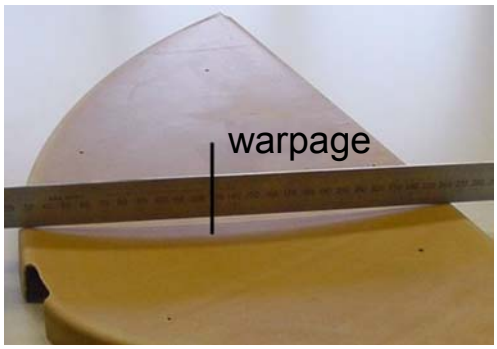

Figure 2. Rib of a wing leader edge showing warpage.

It is difficult to reduce these distortions without altering the forming processes and losing their specific benefit of high production speed. Generally, the narrow tolerances on the product geometry are met by means of costly trial-and-error. Numerical tools such as the Finite Element Method (FEM) have the potential to reduce development costs and scrap material, as well as to optimise the production process used.

This paper considers the warpage of rubber pressed panels consisting of glass weave reinforced poly(phenylene sulphide). The effect of the highly non-isothermal cooling on warping is studied experimentally and numerically, as well as the effect of the mechanical loading on the composite during processing.

2. EXPERIMENTS

Flat panels were subjected to the rubber pressing cycle with flat tools to exclude geometrical effects on the warping of composite panels. Four plies of 8-harness satin glass weave (SS303) and five plies of Hoechst Fortron 214 poly(phenylene sulphide) (PPS) foil, both supplied by Ten Cate Advanced Composites, were stacked as a symmetric and balanced crossply with inplane dimensions of 400×400 mm^2 and a thickness of 0.96 mm. Fine gauged (∅ 0.13 mm) J-type thermocouples were inserted on two opposing sides between the glass plies and at the surface. The glass braid coated thermocouples are able to withstand temperatures up to 400 °C. The stacks were pre-consolidated between steel plates in a Fontyne press at 320 °C under a pressure of 10 bar (1 MPa). After slow and balanced cooling at 5 °C/s to room temperature the laminate was cut in two and disposed of scrap edges using a diamond saw. As a results two flat specimens with inplane dimensions of 180×360 mm^2 containing five thermocouples distributed evenly through the thickness were produced per run.

At Stork Fokker Special Products (Hoogeveen, The Netherlands), the specimens were subjected to the following forming cycle in the rubber press:

- Heating in an infrared oven to a temperature well above the melting temperature (285 °C) of PPS in about 200 seconds;
- Rapid cooling in the closed press under a pressure of about 100 bar (10 MPa) to the release temperature, which can be above the glass temperature of the matrix material. The steel tool is temperature controlled by the oil-heated steel underplate on which it is mounted. The temperature of the rubber tool is not actively controlled;
- Cooling to the room temperature after release from the press and removal from the transport frame.

The silicon rubber tool was designed as a rectangular block with dimensions of 600×300×100 mm^3, the steel tool as a 10 mm thick plate with slightly larger inplane dimensions. The temperature of the thermocouples in the laminate was continuously logged using a data aquisition system and a PC. The logging rate was set to 100 Hz during the step of rapid cooling in the closed press.

The rubber pressed specimens were cut to strips with a lenght-to-width ratio of 15 to exclude any undesirable bistable effects. The geometry of the strips was scanned using a coordinate measurement device. This device consists of two stepper motor controlled sledges for the in-plane (x- and y-directions) movement and a rigidly mounted NCDT laser reflector for non-contact scanning of the specimen's surface in the z-direction normal to the horizontal plane. A second order polynominal $z = a_1x^2 + a_2y^2 + a_3xy + b_1x + b_2y + c$ was fitted through the coordinates, after which the curvature was derived according to:

$$\kappa_x = -\frac{\partial^2 z}{\partial x^2} = -2a_1 \tag{1}$$

Similarly, the curvatures in transverse directions (κ_y, κ_{xy}) were computed and found to be neglible.

3. MODEL DEVELOPMENT

In the recent years, a variety of models has been proposed to analyse the internal stresses that occur during the processing of thermoplastic and thermosetting composite materials and to predict the resulting dimensional changes. Generally, the models comprise the following components: the solution of the heat balance with the process specific thermal boundary conditions; the prediction of changes in the material morphology, such as crystallisation, cure conversion and/or the glass transition; the computation of the stress induced by volumetric changes such as thermal and crystallisation shrinkage. It is recognised that the change in material properties and the resulting change in constitutive behaviour (e.g., viscous to elastic) as a function of the morphology and temperature give rise to "skin-core" effects when a composite solidifies non-isothermally (Månson and Seferis, 1992).

Chapman et al. (1990) computed the inplane residual stresses in a symmetrically cooled carbon/PEEK (polyetheretherketone) composite employing a one-dimensional finite difference method. The temperature and morphology dependent thermoelastic properties of the semicrystalline matrix and thus of the uni-directional plies were computed with micromechanics. A visco-elastic analysis determined the temperature that initiates the transition from viscous to elastic material behaviour. The model was verified with the Process Simulated Laminate (PSL) technique (for example, see Månson and Seferis, 1992) applied to compression

moulded carbon/PEEK laminates which were cooled with 35 ºC/s on the surface. The residual stresses were found to have a magnitude ranging from -40 to 30 MPa for uni-directional laminates.

Lawrence, Månson and Seferis (1992) employed the PSL method to balanced and unbalanced cooled carbon/PEEK laminates. Typically, a 20 ply laminate cooled with 35 ºC/s and 22 ºC/s respectively at the top and bottom, showed a curvature of 1.21 m^{-1} in the 90º direction with a maximum stress of 14.7 MPa.

Recent work by Sunderland, Yu and Månson (2001) reports on the development of a FEM tool to predict the evolution of stresses during the compression moulding of glass fibre reinforced polyetherimide (PEI). A material model that accounts for transitions from viscous to viscoelastic to elastic behaviour was implemented. The influence of balanced and unbalanced cooling at different rates was examined.

Hsiao and Kikuchi (1997) proposed a combined analysis consisting of a FEM analysis of the flow, heat transfer and residual stress evolution during thermoforming of fabric composites and an optimisation algorithm to optimise the process with respect to the laminate thickness. The stresses during the cooling stage are computed instantly elastic below the crystallisation temperature.

Here, an attempt is made to predict the internal stress build-up specifically during rubber pressing with its highly unbalanced thermal and mechanical boundary conditions. The model consists of the components that were mentioned earlier: the heat transfer problem, crystallisation kinetics and the constitutive behaviour of the solidifying composite.

3.1. Heat transfer

Only the cooling stage in the closed press and after pressing is considered, the convection and radiation during heating and transport to and from the press are not taken into account. Then, the heat balance can then be written three-dimensionally as:

$$\vec{\nabla}\cdot\left(\Lambda\cdot\vec{\nabla}T\right)+\dot{q}=\rho C_p\frac{\partial T}{\partial t} \tag{2}$$

where Λ represents the conductivity tensor, $\dot{q}$ is the production of heat per unit of volume, ρ denotes the density and C_p is the heat capacity of the composite. The finite element simulation of the rubber forming process as presented in this paper requires the solution of the one-dimensional heat balance:

$$\lambda_z\frac{\partial^2 T}{\partial z^2}+\dot{q}=\rho C_p\frac{\partial T}{\partial t} \tag{3}$$

assuming that the coefficient of thermal conduction in z-direction λ_z, does not vary spatially. For simplicity, it is assumed that the properties in Equation (3) are independent of the temperature and the crystallinity. The composite thermal properties are obtained by applying simple rules of mixture to the properties of the constituents: a parallel and in-series connection in plane and through the thickness, respectively. The term $\dot{q}$ that accounts for the latent heat that is generated during crystallisation is neglected. Firstly, the heat of fusion for 100% crystalline material is an order of magnitude smaller than the heat capacity times the temperature drop during cooling. Secondly, the mass fraction of crystallising material is small relative to the mass of the total composite.

3.2. Crystallisation kinetics

The current model assumes that solidification of the composite is initiated by the crystallisation of the semi-crystalline matrix material. Also, it takes into account the associated volume change. Crystallisation kinetics are required to predict the formation and growth of the crystalline phase as a function of time and temperature. The isothermal overall bulk crystallisation is analysed using the Avrami equation, see for example Chan and Isayev (1994):

$$\theta=\frac{X_c(t)}{X_{c\infty}}=1-e^{-K(T)t^n} \tag{4}$$

where θ is the relative crystallinity, $X_c(t)$ is the absolute crystallinity at time t and $X_{c\infty}$ is the maximum absolute crystallinity. The rate constant $K(T)$ and the exponent n are retrieved from isothermal crystallisation tests. Extension to a non-isothermal formulation is required for the rubber forming process. The Nakamura (1973) differential model proves to be a useful tool to predict non-isothermal crystallisation using Avrami constants $K(T)$ and n measured under isothermal conditions (Patell and Spruiell, 1991). The Nakamura equation is derived by differentiation and backsubstition of Equation (4) assuming time independency of $K(T)$. It reads:

$$\frac{d\theta}{dt}=nk(T)(1-\theta)\left[-\ln(1-\theta)\right]^{\frac{n-1}{n}} \tag{5}$$

with $k(T)$ related to $K(T)$ in Equation (4) as

$$k(T)=\left[K(T)\right]^{1/n}=(\ln 2)^{1/n}\left(\frac{1}{t_{1/2}}\right) \tag{6}$$

The crystallisation half-time $t_{1/2}$ is defined as the time at which the extent of crystallisation is 50% complete at constant temperature. Patell and Spruiell applied a non-linear regression technique to fit Equation (5) to crystallisation data measured at various cooling rates using the Hoffmann-Lauritzen half-time analysis (Hoffmann et al., 1976). The present model makes use of a more empirical approach of the temperature dependency of $K(T)$. According to Jog and Nadkarni (1985) and Desio and Rebenfeld (1990), $\ln(t_{1/2})$ and subsequently $\ln(K(T))$ are assumed to vary quadratically with the temperature (in °C), or

$$\ln K(T) = aT^2 + bT + c \tag{7}$$

Jog and Nadkarni fitted Equation (7) to isothermally measured crystallisation data of glass-filled PPS (Ryton) obtaining $a = -1.6186 \cdot 10^{-3}$, $b = 0.5505$ and $c = -49.849$. Here, the Nakamura equation is fitted by trial-and-error on the non-isothermal crystallisation data which were measured by Differential Scanning Calorimetry (DSC) at varying cooling rates. The results are shown in Figure 3.

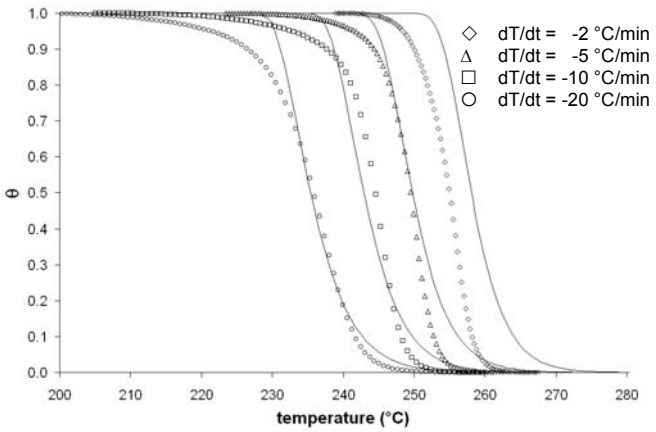

Figure 3. Relative crystallinity vs. the temperature for different cooling rates. The continuous lines represent the simulated results.

The fitted values for a, b, c and the Avrami exponent n are $-1.62 \cdot 10^{-3}$, 0.551, –49.849 and 2.7, respectively. It showed that the numerical results are extremely sensitive to variations in a and n. Regarding the value of the kinetics used, they provide a crude approximation of the development of the crystalline phase. The approach described here needs further and critical evaluation, especially if it is employed for extrapolation to higher cooling rates.

3.3. Constitutive model

A linear viscous-elastic constitutive model is presented that incorporates the viscous to elastic transition of the semi-crystalline matrix material in a highly simplified manner. The viscous matrix is represented as a nearly incompressible elastic solid with a very low Young's modulus $E_{m,viscous}$ above the crystallisation temperature T_c, for example:

$$\begin{aligned} E_{m,viscous} &= \frac{E_m}{1000} \quad T \geq T_c \\ \nu_{m,viscous} &= 0.47 \end{aligned} \tag{8}$$

where $\nu_{m,viscous}$ denotes the Poisson's ratio and E_m is the matrix modulus below T_c. Unlike the model proposed by Chapman et al. (1990), the dependency of these properties on the amount of crystallisation is neglected for simplicity and the lack of appropriate experimental data.

For the same reason the change of the elastic properties due to the glass transition is not considered. Firstly, this is justified somewhat by the observation that the specimens, which were released from the press at temperatures far above the glass transition temperature of PPS (90 °C), already showed significant warpage. Secondly, the cooling from the release temperature to the room temperature takes place by unforced convection and radiation to the surrounding air. It is assumed that this relatively slow and balanced cooling produces no warpage-inducing stresses.

The constitutive behaviour of the composite is modelled using micromechanics on different levels. First, the thermal and elastic properties of a uni-directional ply are calculated from the properties of the temperature-dependent matrix and the fibre by means of micromechanics. The elastic properties of the glass fibre are assumed to be independent of the temperature. Various models are available, of which the Composite Cylinder Assemblage (CCA) by Hashin (1973) is chosen here.

The woven fabric composite is simplified to a symmetric crossply laminate as a first approach. As it is desirable to take into account the through-thickness normal stress and transverse shear stress, the three-dimensional stress-strain relation is required. Goetschel and Radford (1997) and Chen and Tsai (1996) proposed models that yield the thermo-elastic properties of multi-layered composites under the assumption of uniform inplane strains and out-of-plane stresses. Following the work by Goetschel and Radford, Akkerman (2002) recently derived a set of closed-form expressions for the engineering properties of quasi-isotropic laminates.

The averaging method applied in the models mentioned is used here to obtain the constitutive equation of a crossply composite. Consider the stress-strain relation of a uni-directional, transversely isotropic ply in the principal directions (123):

$$\{\sigma_{123}\} = [C]\{\varepsilon_{123}\} \tag{9}$$

The stiffness matrix [C] is the inverse of the commonly known compliance matrix [S]:

$$[C]=[S]^{-1} \tag{10}$$

$$[S]=\begin{bmatrix} \frac{1}{E_1} & \frac{-\nu_{12}}{E_1} & \frac{-\nu_{12}}{E_1} & 0 & 0 & 0 \\ \frac{-\nu_{12}}{E_1} & \frac{1}{E_2} & \frac{-\nu_{23}}{E_2} & 0 & 0 & 0 \\ \frac{-\nu_{12}}{E_1} & \frac{-\nu_{23}}{E_2} & \frac{1}{E_2} & 0 & 0 & 0 \\ 0 & 0 & 0 & 1/G_{23} & 0 & 0 \\ 0 & 0 & 0 & 0 & 1/G_{12} & 0 \\ 0 & 0 & 0 & 0 & 0 & 1/G_{12} \end{bmatrix}$$

The ply properties E_i, ν_i and G_{ij} (i,j =1,2,3) are functions of the isotropic fibre and matrix properties E_f, ν_f, G_f, $E_m(T)$, $\nu_m(T)$ and $G_m(T)$.
The relation in Equation (9) is transformed to the laminate global coordinates by an inplane rotation according to

$$\{\sigma_{xyz}\}=[T][C][T]^T\{\varepsilon_{xyz}\}=[C_{xyz}]\{\varepsilon_{xyz}\} \tag{11}$$

where [T] is the transformation matrix which can be derived using theory of elasticity. A crossply consists of plies stacked at 0° and 90° so the stress-strain relations for the individual layers read

$$\{\sigma_{xyz}\}^{(k)}=[C_{xyz}]^{(k)}\{\varepsilon_{xyz}\}^{(k)}, k=0^\circ,90^\circ \tag{12}$$

Note that $[C_{xyz}]^{(0)}$ equals [C] and $[C_{xyz}]^{(90)}$ is obtained also by switching the first and second rows and colums of [C]. The assumption of uniform inplane strains and uniform through-the-thickness stresses implies

$$\begin{aligned} \varepsilon_i^{(k)}=\varepsilon_i \rightarrow \overline{\sigma}_i=\sum_k V^{(k)}\sigma^{(k)}, \quad i=x,y,xy \\ \sigma_j^{(k)}=\sigma_j \rightarrow \overline{\varepsilon}_j=\sum_k V^{(k)}\varepsilon^{(k)}, \quad j=z,yz,xz \\ k=0^\circ,90^\circ \end{aligned} \tag{13}$$

where $V^{(k)}$ = 1/2 is the volume fraction of plies with equal orientation. Solving Equations (12) and (13) yields the averaged constitutive equation for a crossply laminate

$$\begin{Bmatrix} \overline{\sigma}_x \\ \overline{\sigma}_y \\ \overline{\sigma}_z \\ \overline{\sigma}_{yz} \\ \overline{\sigma}_{xz} \\ \overline{\sigma}_{xy} \end{Bmatrix}=\begin{bmatrix} \overline{C}_{11} & \overline{C}_{12} & \overline{C}_{13} & 0 & 0 & 0 \\ \overline{C}_{12} & \overline{C}_{11} & \overline{C}_{13} & 0 & 0 & 0 \\ \overline{C}_{13} & \overline{C}_{13} & \overline{C}_{33} & 0 & 0 & 0 \\ 0 & 0 & 0 & \overline{C}_{44} & 0 & 0 \\ 0 & 0 & 0 & 0 & \overline{C}_{44} & 0 \\ 0 & 0 & 0 & 0 & 0 & \overline{C}_{66} \end{bmatrix}\begin{Bmatrix} \overline{\varepsilon}_x \\ \overline{\varepsilon}_y \\ \overline{\varepsilon}_z \\ \overline{\varepsilon}_{yz} \\ \overline{\varepsilon}_{xz} \\ \overline{\varepsilon}_{xy} \end{Bmatrix} \tag{14}$$

with

$$\begin{aligned} \overline{C}_{11} &= \frac{1}{2}(C_{11}+C_{22})-\frac{1}{4}\frac{(C_{12}-C_{23})^2}{C_{22}} \\ \overline{C}_{12} &= C_{12}+\frac{1}{4}\frac{(C_{12}-C_{23})^2}{C_{22}} \\ \overline{C}_{13} &= \frac{1}{2}(C_{12}+C_{23}) \\ \overline{C}_{33} &= C_{22} \\ \overline{C}_{44} &= \frac{1}{2}\frac{C_{44}C_{66}}{C_{44}+C_{66}} \\ \overline{C}_{66} &= C_{66} \end{aligned} \tag{15}$$

where it is assumed that the laminate is stacked balanced and symmetrically. Equation (15) does not take into account the contribution of the separate plies to the bending stiffness.
The model can easily be extended to include the thermal shrinkage and the volume change due to crystallisation. The averaged coefficients of thermal expansion (CTE's) are readily available from Akkerman's (2002) quasi-isotropic modelling - the CTE's of a crossply equal the CTE's of a quasi-isotropic composite because +45°/- 45° plies give no different contribution to the laminate CTE than 0°/90° plies. The averaged CTE's are formulated in terms of the ply properties as

$$\begin{aligned} \alpha_x=\alpha_y &= \frac{(E_1+\nu_{12}E_2)\alpha_1+(1+\nu_{12})E_2\alpha_2}{E_1+(1+2\nu_{12})E_2} \\ \alpha_z &= \frac{(\nu_{12}E_2-\nu_{23}E_1)\alpha_1+((1+\nu_{23})E_1+(1+\nu_{12})E_2)\alpha_2}{E_1+(1+2\nu_{12})E_2} \end{aligned} \tag{16}$$

The ply properties α_1 and α_2 are calculated from the matrix and fibre CTE, respectively α_m and α_f using micromechanics. The latter two are assumed to be independent of the temperature. The crystallisation shrinkage is derived similarly. The complete stress-strain relationship is now written as

$$\{\overline{\sigma}\}=[\overline{C}]\{\overline{\varepsilon}-\overline{\alpha}\Delta T-\overline{\beta}\theta\} \tag{17}$$

where the vector $\{\beta\}$ denotes the total crystallisation shrinkage, θ is the relative amount of crystallisation

known from Equation (5) and ΔT represents a temperature change.
The effect of the Young's modulus of the matrix E_m on several coefficients of $[\overline{C}]$ is illustrated in Figure 4.

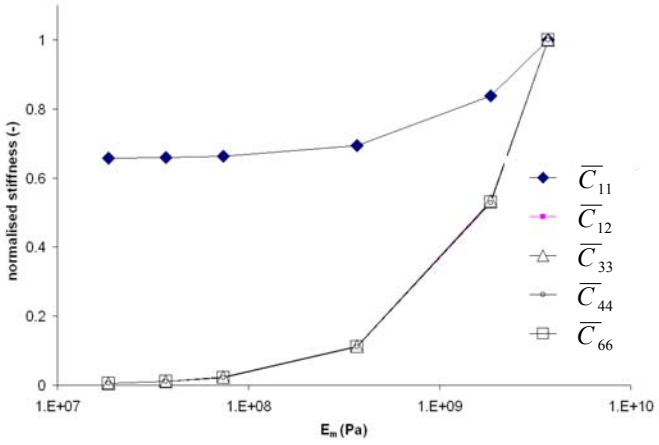

Figure 4. The influence of the matrix modulus on the stiffness coefficients in Equation (14)

The coefficients $\overline{C}_{11}$, $\overline{C}_{12}$, $\overline{C}_{33}$, $\overline{C}_{44}$ and $\overline{C}_{66}$ are plotted against the modulus E_m. The last four coefficients coincide in the figure. All are normalised with their values calculated with an E_m of 4 GPa, which is the modulus of PPS at room temperature. Obviously, the matrix dominated coefficients $\overline{C}_{33}$, $\overline{C}_{44}$ and $\overline{C}_{66}$, respectively representing E_z, G_{13} and G_{12}, drop considerably when E_m decreases. The coeffcient $\overline{C}_{11}$, which is a measure for the inplane stiffness E_x, depends strongly on the modulus of the fibre and consequently decreases not further than about 65% of its initial value.
Recapitulating, the concept of modelling the matrix material as an elastic solid with a low modulus above the crystallisation temperature results in a composite that cannot sustain transverse shear deformation, but remains fairly stiff in the fibre direction above the crystallisation temperature.

3.4. *FE implementation*

The material model has been implemented in DiekA (Huétink, 1990), an in-house developed FE package. The weak forms of the stress equilibrium equations and heat balance are solved incrementally by means of the updated Langrange method. It requires the discretisation of the stress-strain relation in time:

$$\{\Delta\sigma\} = [\overline{C}]\{\Delta\varepsilon - \overline{\alpha}\Delta T - \overline{\beta}\Delta\theta\} \qquad (18)$$

where it is assumed that the change of the stiffness during solidification causes no stress.

4. RESULTS AND DISCUSSION

4.1. Experimental results

The preconsolidated specimens were subjected to the rubber pressing cycle with the steel tool set at different temperatures of 100 °C, 160 °C and 200 °C. The other process parameters such as reheating time and temperature, pressure and consolidation time remained unchanged. The uncontrolled surface temperature of the rubber tool was probed before each cycle. A set of five specimens was pressed at each steel tool temperature, of which three were equipped with thermocouples. An extra set of experiments was added by adhering a layer of Tygaflor (glass weave reinforced PTFE) with a thickness of 0.2 mm onto the steel tool with the purpose of investigating its influence on the heat transfer and mechanical loading. The curvatures resulting from the different tests are depicted in Figure 5. Note that a positive curvature represents a concave shaped laminate.

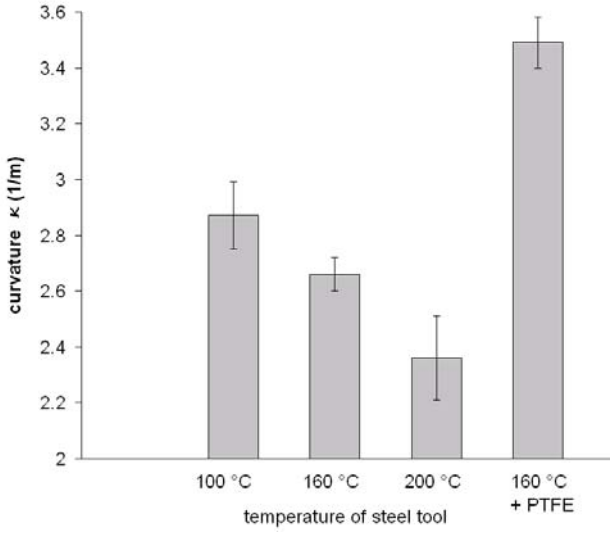

Figure 5. Measured curvature of specimens pressed at different temperatures of the steel tool

A first glance at the results seems to confirm the skin-core theory that describes how internal stresses build up due to a thermal gradient through the laminate thickness in combination with a change in material stiffness. As a rule of thumb it can be stated that the faster cooling material builds up a compressive stress while the material that cools slower is subjected to a tensile stress. Primarily, it is assumed that the cooling on the rubber tool side of the composite is slow compared to the steel tool side due to the poor thermal conductivity of the rubber. Hypothetically, as the temperature of the steel tool increases, the heat transfer from the composite to that tool decreases resulting in a more balanced cooling profile. Following this reasoning the stress profile

through the thickness becomes more symmetrical, and thus the final curvature smaller.
However, the curvature dramatically increases from 2.66 m^{-1} to 3.49 m^{-1} when a layer of Tygaflor is applied to the steel tool at 160 °C. This observation does not match the hypothesis above; the cooling to the steel side decreases as a result of the low thermal conductivity of the Tygaflor, but the composite plate shows a larger curvature. A plot of the evolution in time of the temperature profile seems to invalidate the hypothesis further, see Figure 6.

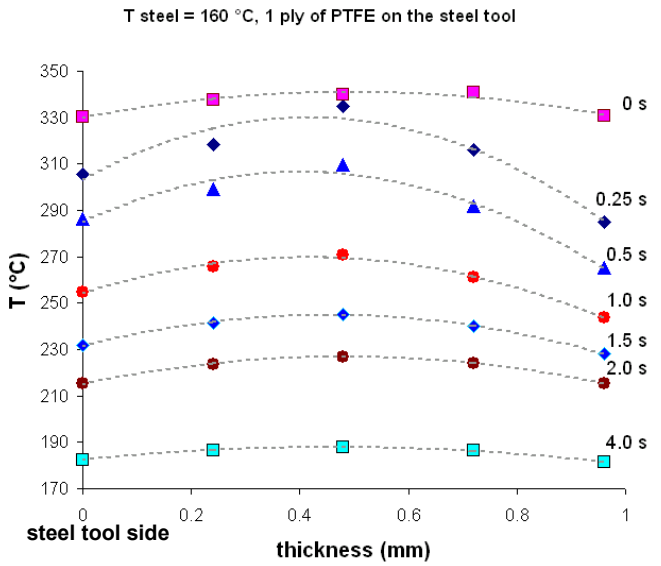

Figure 6. Cooling through the thickness of the laminate with the steel tool set to 160 °C and coated with Tygaflor.

It shows that the cooling is rather symmetrical and nearly uniform in the temperature range of 200-240 °C where crystallisation occurs. It can be expected that this thermal history results in low internal stress levels which cause no warping of the composite laminates at room temperature. Therefore, it appears to be very likely that more mechanisms drive the warpage of these laminates. One of these mechanisms might be the difference in contact conditions imposed on the composite during consolidation. Stick or slip in the interphases of the composite with the tooling can cause the build-up or release of stress, respectively. The influence of these conditions and the effect of tool temperature on the warpage of the composite panels are treated numerically in the next session.

4.2. Numerical results

The rubber pressing of the glass/PPS composite is modelled two-dimensionally as a first approach, using linear 4 node plane strain elements. A sketch of the problem is shown in Figure 7.

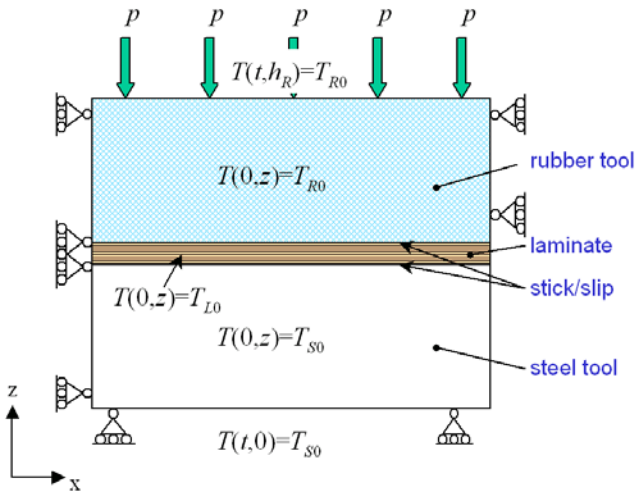

Figure 7. Schematic representation of the FE simulations.

Symmetry boundary conditions are imposed on the left hand side. The right hand side displacements in x-direction (u_x) of the rubber tool are suppressed as the tool is enclosed by a steel box. The steel tool is able to expand freely. Thermally, the right hand side is restrained from heat transfer to the environment, which consequently reduces the thermal problem to a one-dimensional case.
The convection and radiation of heat during transport from the oven to the press are neglected; the temperatures of the steel tool and the laminate, respectively T_{S0}, and T_{L0}, are assumed to be uniform at the start of the cooling cycle. In the actual process, the rubber tool is shortly pre-heated on the steel tool. This step is taken into account in the simulations, resulting in different surface temperatures of the rubber tool for different steel tool temperatures. The top and bottom side of respectively the rubber and steel tool are modelled as insulated walls.
The pressure is applied on the top side of the rubber block. Regarding the displacements in z-direction (u_z), the top and bottom side of the composite are coupled with the opposing faces of the tools. The displacements u_x of the composite are controlled by assuming stick or slip conditions on contact with the tools.
The simulated cooling history of the composite midplane is compared to the measurements in Figure 9 to demonstrate the accuracy of the simulations. The largest deviations occurred at the top and bottom of the laminate, but they remained within 7%.

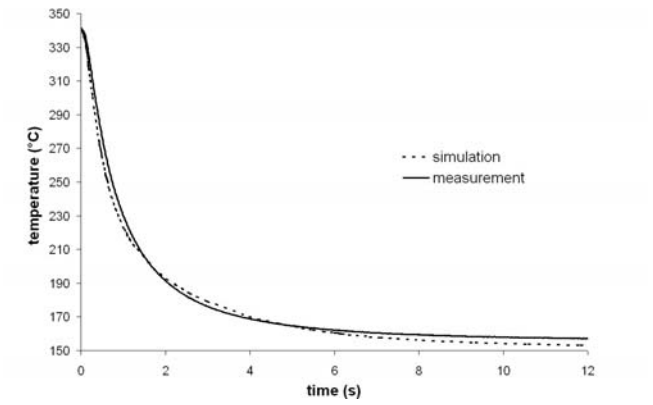

Figure 8. Simulated and measured temperature history of the midplane of the laminate during rubber pressing with the steel tool set to 160 °C.

The curvatures computed with the steel tool set to 100 °C, 160 °C and 200 °C and using different stick and slip conditions are shown in Figure 9.

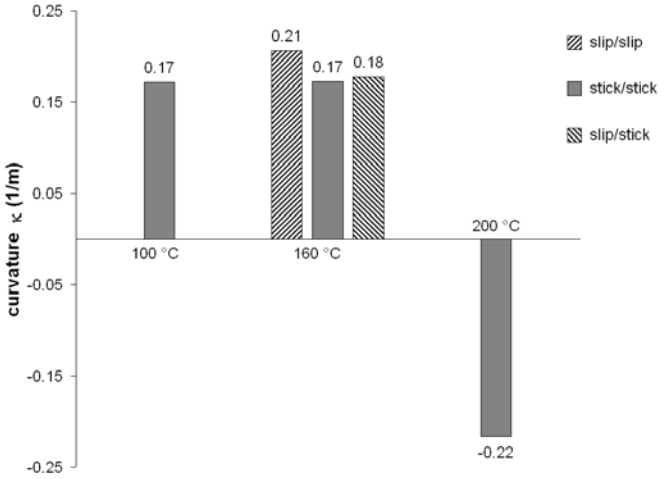

Figure 9. Computed curvature as a result of a varying temperature of the steel tool. The influence of stick or slip conditions on the interfaces of the laminate with the steel and rubber tool is shown for the 160 °C case.

Obviously, the numerical results deviate considerably from the measured curvatures as presented in Figure 5. The first are an order of magnitude smaller than the latter. The difference between the curvatures simulated with the temperature of the steel tool set to 100 °C and 160 °C appears to be negligible. This is a consequence of the pre-heating of the rubber tool by pressing it onto the steel tool; if the set temperature of the latter increases, the surface temperature of the rubber tool increases likewise. Although the average cooling rate in the laminate decreases, the cooling profile through the thickness retains a more or less equal shape. Consequently, the same effect is seen with the resulting residual stresses. Figure 10 shows a plot of the distribution of the normal stress σ_x through the thickness of the laminate before it is released from the moulds.

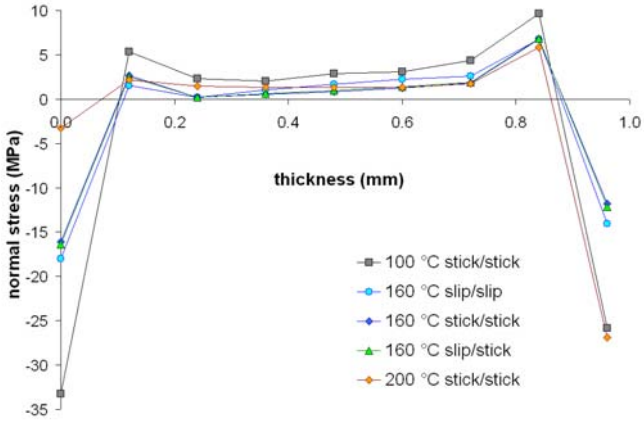

Figure 10. Inplane normal stress through the thickness of the laminate before release.

It shows that the "skin"-stresses are larger in the 100 °C than in the 160 °C case but the stress profiles are shaped equally. The difference in the moment that induces curvature according to

$$\kappa = \frac{M}{E_x I} = \frac{1}{E_x I}\int_{-h/2}^{h/2} \sigma_x z dz \qquad (19)$$

will therefore be small. In Equation (19), E_x and I denote the inplane stiffness and moment of inertia, respectively, and h is the laminate thickness.
From Figure 10 it shows that the sign of the curvature changes when the temperature of the steel tool is set to 200 °C. Although the rubber tool is pre-heated to a higher temperature than in the two other cases, the cooling was found to be faster on the rubber tool side. The stress profile in Figure 10 shows that the compressive stress on the steel tool side is considerably smaller than on the rubber tool side. Consequently, the laminate becomes convex shaped.

The thermal history through the thickness combined with a change in stiffness due to solidification causes a build-up of internal stresses, but evidently these are not large enough to warp the laminate as much as observed experimentally.
The choice for stick or slip conditions between the tools and the laminate has an effect on the simulated curvature. However, the effect is not significant enough to approximate the experimental results and to account for the observed influence of a ply of Tygaflor on the steel tool.
In all cases the stress levels remain low in the order of 1 MPa in the centre and 10-30 MPa in the outer plies. When the CLT is applied to compute the internal stress distribution that occurs when a 0.96 mm thick crossply is bent to a curvature of 3 m^{-1}, it shows that the stress reaches a maximum of + and - 40 MPa in the top and bottom ply, respectively. Somehow, a large amount of stress builds up during rubber pressing that cannot be

accounted for with the skin-core theory. A possible mechanism is demonstrated in the following paragraph.

4.3. Frozen-in deformation

The ± 1 mm thick laminate penetrates the rubber tool when the press is closed. High stress concentrations therefore exist near the edges of the laminate. It is well imaginable that the top ply is pulled over the underlying plies as sketched in Figure 11 and that the laminate is thereby subjected to a considerable shear strain.

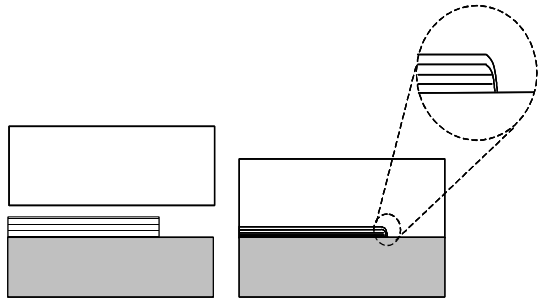

Figure 11. Transverse shear induced by penetration.

The edges of the rubber pressed specimens show this transverse shearing as can be viewed in a microscopic picture, see Figure 12.

Figure 12. Microscopic picture of an edge of a rubber pressed specimen. The bundles in warp direction have been highlighted.

Consider the response of a laminate that is subjected to transverse shear in its viscous state as depicted in Figure 13.

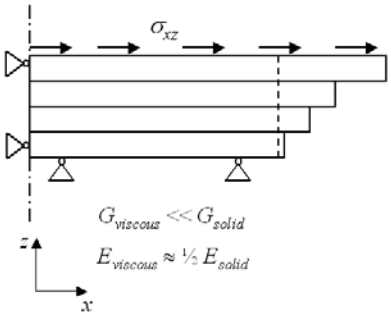

Figure 13. Transverse shearing of a laminate with interply slip

In paragraph 4.3, it showed that the shear stiffnesses drop considerably but that the inplane tensile modulus remains fairly high at temperatures above the crystallisation temperature. Then, subjecting the material to transverse shear deformation in its viscous state is comparable to straining the plies separately. When the material solidifies, which causes a dramatical increase of the transverse shear stiffness, the plies are "bonded" together and the ply-strains are frozen in. The resulting stress is relieved by curvature of the laminate.
FE simulations clearly demonstrate this effect. The case with the temperature of the steel tool set at 160 °C was repeated, but with an additional shear deformation. This deformation was applied by prescribing the displacements of the nodes on the top side of the composite, thereby subjecting that side to a tensile strain of 0.5%. Stick conditions were imposed on the bottom side. The normal stresses before vertical release of the laminate are plotted against the thickness coordinate in Figure 14.

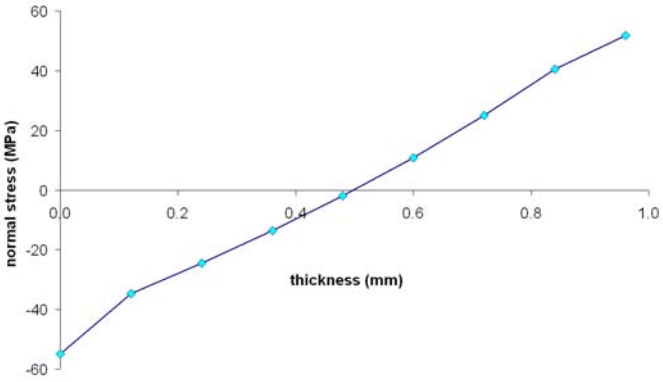

Figure 14. Through-thickness normal stress before release as a result of frozen-in transverse strain.

The resulting curvature was computed as 3.87 m^{-1}, which is in the same order of magnitude as the experimentally obtained curvatures.
The shear deformation was applied "manually" in the example. FE simulations of the penetration of the rubber tool are required to check the actual response of the laminate and the tool.

5. CONCLUSIONS

An experimental and a numerical study have been performed to measure and simulate the warpage of glass fibre reinforced PPS panels that were formed with the rubber forming process. A material model has been proposed that incorporates the solidification of the semi-crystalline matrix material. Finite Element simulations showed that the thermal gradient through the thickness during consolidation, in combination with the change in stiffness of the composite has a minor contribution to the build up of internal stresses. Consequently, it is concluded that another mechanism drives the warpage

of the panels. It is suggested that transverse shear deformation is frozen in, which is demonstrated with a numerical example.

ACKNOWLEDGEMENTS

The authors wish to acknowledge gratefully the support of Ten Cate Advanced Composite, Stork Fokker Special Products and the Netherlands Agency for Aerospace Programmes.

REFERENCES

Akkerman, R., 2002, "On the properties of quasi-isotropic laminates", Composites Part B: Engineering, vol.33: pp.133-140.

Chan, T.W. and Isayev, A.I., 1994, "Quiescent polymer crystallization: Modeling and measurements", Polymer Engineering and Science, vol.34(6):pp.461-471.

Chapman, T.J., Gillespie Jr., J.W., Pipes, R.B., Månson, J-A.E. and Seferis, J.C., 1990, "Prediction of process-induced residual stresses in thermoplastic composites", Journal of Composite Materials, vol.24: pp.616-642.

Chen, H.J. and Tsai, S.W., 1996, "Three-dimensional effective moduli of symmetric laminates", Journal of Composite Materials, vol.30(8): pp.906-917.

Desio, G.P. and Rebenfeld, L., 1990, "Effects of fibers on the crystallization of poly(phenylene sulfide)", Journal of Applied Polymer Science, vol.39: pp.825-835.

Goetschel, D.B. and Radford, D.W., 1997, "Analytical development of through-thickness properties of composite laminates", Journal of Advanced Materials, vol.28(4):pp. 37-46.

Hashin, Z., "Analysis of composite materials", Journal of Applied Mechanics, vol.50: pp. 481-.

Hoffmann, J.D., Davis, G.T. and Lauritzen, J.I., 1976, "Treatise on solid state chemistry: Crystalline and non-crystalline solids (vol.3)", New York, Plenum, ISBN 0-306-35053-X.

Hsiao, S.W. and Kikuchi, N., 1997, "Numerical analysis and optimal design of composite thermoforming process", Computer Methods in Applied Mechanics and Engineering, vol. 177: pp.1-34.

Huétink, J., Vreede, P.T. and Van der Lugt, J., 1990, "Progress in mixed Eulerian-Langrangian finite element simulation of forming processes", International Journal of Numerical Methods in Engineering, vol.30: pp.1441.

Jog, J.P. and Nadkarni, V.M., 1985, "Crystallization kinetics of polyphenylenesulphide", Journal of Applied Polymer Science, vol.39: pp.997-1009.

Lawrence, W.E., Månson, J-A.E., and Seferis, J.C., 1992, "Thermal and morrphological skin-core effects in processing of thermoplastic composites", Composites, vol.21(6):pp.475-480.

Månson, J-A.E. and Seferis, J.C., 1992, "Process Simulated Laminate (PSL): A methodology to internal stress characterisation in advanced composite materials", Journal of Composite Materials, vol.26(3): pp.405-431.

Nakamura, Y.P., Katayama, K. and Amano, T., 1973, "Some aspects of non-isothermal crystallization of polymers. II. Consideration of the isokinetic condition", Journal of Applied Polymer Science, vol.17: pp.1031-1041.

Patel, R.M. and Spruiell, J.E, 1991, "Crystallization kinetics during polymer processing - analysis of available approaches for process modeling", Polymer Engineering and Science, vol.31(10): pp.730-738

Sunderland, P., Yu, W. and Månson, J-A.E., 2001, "A thermoviscoelastic analysis of process-induced internal stresses in thermoplastic matrix composites", Polymer Composites, vol.22(5): pp.579-592.